Spin-orbit coupling effects on the superfluidity of a Fermi gas in an optical lattice

Q. Sun,[1,2] G.-B. Zhu,[3] W.-M. Liu,[2] and A.-C. Ji[1,*]

[1]*Department of Physics, Capital Normal University, Beijing 100048, China*

[2]*Institute of Physics, Chinese Academy of Sciences, Beijing 100190, China*

[3]*Department of Physics and Materials Science, City University of Hong Kong, Tat Chee Avenue, Kowloon, Hong Kong, China*

(Received 19 April 2013; revised manuscript received 29 November 2013; published 23 December 2013)

We investigate the superfluidity of attractive Fermi gas in a square optical lattice with spin-orbit coupling (SOC). We show that the system displays a variety of new features. At half filling, SOC induces a Dirac semimetal and the system undergoes a semimetal-superfluid transition. Near half filling, we find that the superfluidity tends to be suppressed due to the emerging Dirac cones. While for small fillings, SOC can induce a BCS-BEC crossover beyond the conventional attractive Hubbard model, which is characterized by a bound state in the lattices. Moreover, we demonstrate that the superfluid density also exhibits many unusual properties in the lattices.

DOI: 10.1103/PhysRevA.88.063637 PACS number(s): 03.75.Ss, 67.85.Lm, 05.30.Fk, 37.10.Jk

I. INTRODUCTION

The spin-orbit coupling (SOC) plays a central role in the search for novel topological states in solid state physics [1,2]. This has stimulated tremendous interests in creating artificial non-Abelian gauge fields in ultracold atom systems [3]. The successful realization of SOC in both Bose-Einstein condensate (BEC) [4–6] and Fermi gas [7,8] opens up a new avenue towards studying the rich physics of spin-orbit (SO) -coupled ultracold atoms [9–13]. One of the important advances is that SOC was shown to have fundamental effects on the superfluidity of continuous Fermi gases [14–20].

On the other hand, remarkable progress has been made to simulate the Fermi-Hubbard model using ultracold atoms loaded into an optical lattice [21,22] to address the most challenging problems [23]. In particular, the simulation and investigation of attractive Hubbard model [24] has attracted special interests for the superfluidity of fermionic atoms away from resonance [25–28], which is also a basic model for many superconducting materials [29]. Recently, SOC has been combined with the optical lattices to study many interesting physics for the repulsive Hubbard model [30–32]. Nevertheless, the superfluidity of SO-coupled lattices for attractive Fermi gas remains a new frontier to be explored.

In this paper, we shall focus on the Hubbard regime of a Fermi gas in a square optical lattice with SOC. Such a system can be described by a generalized negative-U Hubbard model. We show that, the introduction of SOC into the lattices makes this system differ entirely from the continuum models and gives rise to a variety of new features. First, SOC in a square optical lattice can induce four Dirac cones, which offers a unique system to study the superfluidity of a semimetal, where we predict the existence of a semimetal-superfluid transition with $U_c/t \simeq 3.11$ for large SOC at half filling. We find that while the superfluidity tends to be suppressed due to the emerging Dirac cones near half filling, SOC can lead to a BCS-BEC crossover beyond the conventional attractive Hubbard model for small fillings, which is characterized by a bound state in the lattices. Such an evolution from SOC-induced Dirac superfluidity to the BCS-BEC crossover makes this system an ideal playground for the investigation of emerging physics in the Fermi-Hubbard model. Moreover, the superfluid density also presents many unusual features in this SO-coupled optical lattice.

This paper is organized as follows: We first present the model and discuss the single-particle spectrum in Sec. II. Then in Sec. III, we derive the formulation and the effective spin model via the strong-coupling expansion. In Sec. IV, we analyze the pairing gap and phase transitions at zero temperature. Also, we discuss the finite-temperature phase, which is important for real experiments. After that, we investigate the SOC effects on the condensate and superfluid densities in the lattices in Sec. V. Finally the experimental feasibility of actual realization of the system is discussed in Sec. VI.

II. THE MODEL AND ENERGY SPECTRUM

We consider a two-component Fermi gas subject to an optical square lattice. In the tight-binding approximation, the Hamiltonian of the system reads

$$H = -t\sum_{\langle ij\rangle}\sum_{\sigma\sigma'}(c^{\dagger}_{i\sigma}R_{ij}c_{j\sigma'} + \text{H.c.}) - U\sum_{i} n_{i\uparrow}n_{i\downarrow} - \mu\sum_{i} n_i, \quad (1)$$

where t is the overall hopping amplitude and $c^{\dagger}_{i\sigma}$ is the creation operator for spin-up (down) fermion $\sigma = \uparrow,\downarrow$ at site i. The nearest sites tunneling matrices $R_{ij} = e^{i\vec{A}\cdot(\vec{r}_j-\vec{r}_i)}$ with $\vec{A} = \lambda(\sigma_x,\sigma_y)$ the non-Abelian gauge field [30–33], and λ is the strength of Rashba SOC [34] [see Fig. 1(a)]. Here, the diagonal term of R_{ij} denotes the spin-conserved hopping, while the nondiagonal term can be realized by the Raman laser-assisted spin-flipped tunneling [35]. U is the on-site attraction strength which can be tuned by Feshbach resonances and μ is the chemical potential. $n = \langle n_{i\uparrow} + n_{i\downarrow}\rangle$ is the filling factor.

Figure 1(b) shows the band structure of noninteracting fermions, where SOC lifts the spin degeneracy and gives rise to two split Rashba bands. Remarkably, the two bands intersect linearly at $\Gamma = (0,0)$, $M = (\pi,0),(0,\pi)$, and $K = (\pi,\pi)$. The zero energy Fermi surfaces at half filling are shown in Fig. 1(c),

*andrewjee@sina.com

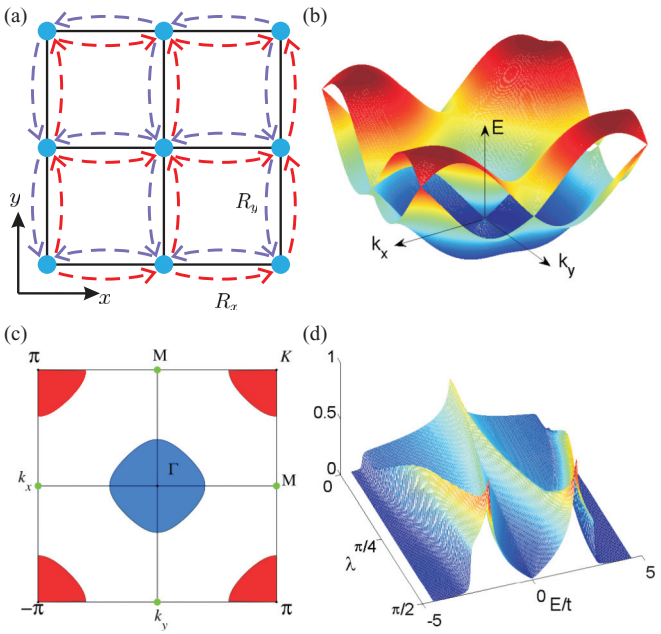

FIG. 1. (Color online) (a) SO-coupled square optical lattice, where $R_{x(y)}$ denotes the non-Abelian hopping matrix along $x(y)$ direction. (b) Energy bands of noninteracting fermions with $\lambda = 3\pi/10$ for illustration. (c) Zero energy Fermi surfaces at half filling, where the filled particle (blue) and hole (red) Fermi pockets represent the up and down Rashba bands, respectively. The green dots denote two zero energy Fermi points at M. (d) Density of states $\rho(E)$ for $\lambda \in [0,\pi/2]$.

where we have a particle (hole) Fermi pocket around Γ (K) which is associated to the up (down) Rashba band, respectively. Note that there always exist two zero energy Fermi points located at M for any $\lambda \neq 0$. Specifically, when $\lambda = \pi/2$, both the particle (hole) Fermi pockets shrink to Fermi points at zero energy, and there develops a semimetal with four Dirac cones at Γ, K, and M. Figure 1(d) shows the density of states (DOS) $\rho(E)$ of single-particle excitation over the regime $\lambda \in [0,\pi/2]$; we see that when $\lambda = \pi/2$, $\rho(E) \propto |E|$, which vanishes linearly around zero energy.

III. THE FORMULATION AND STRONG-COUPLING ANALYSIS

We write the partition function of Eq. (1) as $\mathcal{Z} = \int \mathcal{D}[\bar{\psi},\psi] e^{-S[\bar{\psi},\psi]}$ with $S[\bar{\psi},\psi] = \int_0^\beta d\tau [\sum_\sigma \bar{\psi}_\sigma \partial_\tau \psi_\sigma + H(\bar{\psi},\psi)]$. Then, by decoupling the attractive term in normal and anomalous channels through a pairing field $\Delta_i(\tau) = U\psi_{i\downarrow}(\tau)\psi_{i\uparrow}(\tau)$, we can obtain the effective action $S_{\rm eff} = \sum_i \int_0^\beta d\tau \frac{|\Delta_i(\tau)|^2}{U} - \frac{1}{2}\mathrm{Tr}\ln\mathcal{G}^{-1} + \beta\sum_{\mathbf{k}}\varepsilon_{\mathbf{k}}$. Here the inverse Green function is given by

$$\mathcal{G}^{-1} = \begin{pmatrix} \partial_\tau + \varepsilon_{\mathbf{k}} + \lambda_{\mathbf{k}} & -i\sigma_y\Delta_i(\tau) \\ i\sigma_y\bar{\Delta}_i(\tau) & \partial_\tau - \varepsilon_{\mathbf{k}} + \bar{\lambda}_{\mathbf{k}} \end{pmatrix}, \tag{2}$$

with $\varepsilon_{\mathbf{k}} = -2t\cos\lambda(\cos k_x + \cos k_y) - \bar{\mu}$ and $\lambda_{\mathbf{k}} = -2t\sin\lambda(\sin k_x\sigma_x + \sin k_y\sigma_y)$, $\bar{\lambda}_{\mathbf{k}}$ is the complex conjugate of λ_k, and $\bar{\mu} = \mu + Un/2$ is the scaled chemical potential. Furthermore, we set $\Delta_i(\tau) = \Delta + \delta\Delta$ and write $\mathcal{G}^{-1} = G^{-1} + \Sigma$ with $G^{-1} = \mathcal{G}^{-1}|_{\Delta_i(\tau)=\Delta}$, and Σ represents the fluctuation $\delta\Delta$ of the pairing field. Then, to the second order of Σ, the effective action can be expanded as $S_{\rm eff} \simeq S_0 + \Delta S$ with $S_0 = \frac{\beta N}{U}\sum|\Delta|^2 + \frac{1}{2}\sum_{\mathbf{k},\nu=\pm}[\frac{\beta}{2}(\varepsilon_{\mathbf{k}} - E_{\mathbf{k},\nu}) - \ln(1+e^{-\beta E_{\mathbf{k},\nu}})]$, and $\Delta S \equiv \sum_q \Gamma^{-1}(q)\delta\bar{\Delta}(-q)\delta\Delta(q) = \frac{N}{U}\sum_q \delta\bar{\Delta}(-q)\delta\Delta(q) + \frac{1}{4}\mathrm{Tr}[\mathrm{G}(k)\Sigma(-q)\mathrm{G}(k-q)\Sigma(q)]$. Here $k = (\mathbf{k}, iw_n)$, $q = (\mathbf{q}, i\nu_n)$, and $E_{\mathbf{k},\pm} = \sqrt{\xi^2_{\mathbf{k},\pm} + \Delta^2}$ with $\xi_{\mathbf{k},\pm} = \varepsilon_{\mathbf{k}} \pm 2t\sin\lambda\mathcal{K}$ being the two Rashba branches, $\mathcal{K} \equiv \sqrt{\sin^2 k_x + \sin^2 k_y}$. At the mean-field level, the many-body ground state of the system can be derived by minimizing $S_0/(N\beta)$ with respect to Δ and μ, and we have the following gap and Fermi density equations:

$$\begin{aligned} \frac{1}{U} &= \frac{1}{N}\sum_{\mathbf{k},\nu=\pm}\frac{1}{4E_{\mathbf{k},\nu}}\tanh\left(\frac{\beta E_{\mathbf{k},\nu}}{2}\right), \\ n &= 1 - \frac{1}{N}\sum_{\mathbf{k},\nu=\pm}\frac{\varepsilon_{\mathbf{k}}}{2E_{\mathbf{k},\nu}}\tanh\left(\frac{\beta E_{\mathbf{k},\nu}}{2}\right). \end{aligned} \tag{3}$$

To proceed, it's beneficial to consider the large attraction limit with $U/t \gg 1$ in such a lattice model. In this case, we can explore the strong-coupling expansion for Eq. (1) through the canonical transformation $c_{i\uparrow} \to c_{i\uparrow}$ and $c_{i\downarrow} \to (-1)^{i_x+i_y}c^\dagger_{i\downarrow}$ [36]. For any band filling, we derive an effective spin model

$$H_{\rm spin} = J\sum_{\langle ij\rangle}\mathbf{S}_i\cdot\mathbf{S}_j - 2\bar{\mu}\sum_i S^z_i, \tag{4}$$

with $J = 4t^2/U$, where the pairing field operator becomes the transverse magnetic operator. Surprisingly, we find that Eq. (4) applies for *arbitrary SOC*, and the system favors an antiferromagnetic order in the XY plane for $\bar{\mu} \neq 0$, which is equivalent to the pairing order of Eq. (1). This means that, in the large U limit, SOC has little influence on the superfluidity of the system, because all the fermionic atoms form tightly bound molecules and give rise to a Kosterlitz-Thouless (KT) transition of BEC. Whereas, in the weak and intermediate attraction regions, SOC introduces fundamental effects into the lattices as shown below.

IV. THE PAIRING GAP AND PHASE TRANSITIONS

The pairing gaps at zero temperature are illustrated in Fig. 2. First for half filling ($n = 1$), Fig. 2(a) shows that the BCS gap decreases monotonically with respect to λ. This could be understood that, the Fermi pockets around Γ and K [see Fig. 1(c)] tend to form the Fermi points at $E_F = 0$ by increasing SOC, which causes a suppression of DOS at zero energy [see Fig. 1(d)]. Specifically, when $\lambda = \pi/2$ the system becomes a semimetal, which is expected to be stable towards small attractions. On the other hand, when $U/t \gg 1$ the system should support a superfluid state of bound molecules as indicated by the effective spin model of Eq. (4) [37]. Hence, there must undergo a significant quantum phase transition (QPT) from a semimetal to a superfluid by increasing attractions [see the thick vertical line of Fig. 2(a).] In the inset, we show that the critical value $U_c/t \simeq 3.11$. Such a QPT should be observed close to $\lambda = \pi/2$, where a finite gap develops above U_c/t.

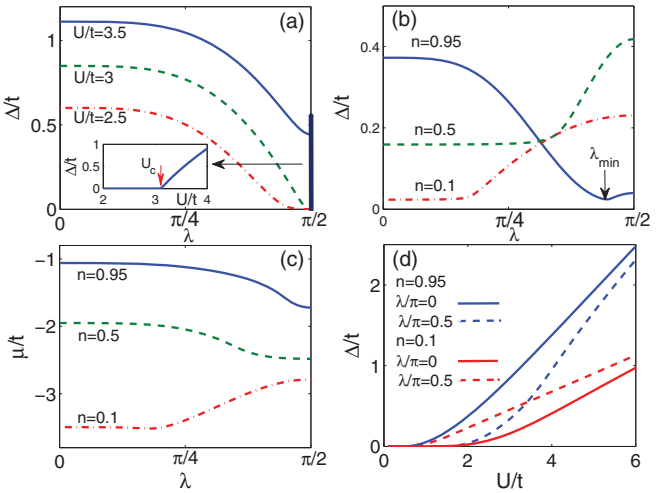

FIG. 2. (Color online) (a) Plot of Δ versus λ at half filling for different U/t. Inset shows a semimetal-superfluid QPT with $U_c/t \simeq 3.11$. (b) Plot of Δ and (c) μ versus λ with $U/t = 2$ for different fillings. (d) Pairing gap as a function of U/t for two typical fillings with $n = 0.1$ (red) and 0.95 (blue). Solid and dashed lines represent $\lambda = 0$ and $\pi/2$, respectively.

The situation would change remarkably upon dopings, as shown in Fig. 2(b). Without loss of generality, we focus on the hole doping case due to the particle-hole symmetry of the system. First for small dopings, similar to that of half filling, the superfluidity is governed by emerging Dirac cones at zero energy and Δ is suppressed by increasing λ (see $n = 0.95$). However, when close to $\lambda = \pi/2$, the doping would make the QPT at half filling unstable and opens a gap. This produces a nonmonotonic behavior of Δ with a minimum at $\lambda_{\min}$, while for large dopings, the influence of Dirac cones would diminish. In this case, we find that SOC induces a BCS-BEC crossover, which is characterized by Δ being significantly enhanced (see $n = 0.1$). To understand this point, we solve the two-body problem of Eq. (1), which is determined by $\Gamma^{-1}(i\nu_n \to \omega + i0^+, \mathbf{q} = 0) = 0$ as $\omega + 2\bar{\mu} = -E_B$ and we arrive at

$$\frac{1}{U} = \frac{1}{2}\int_{E_0}^{|E_0|} \frac{\rho(E)dE}{2E + (|E_B| - 2E_0)}, \tag{5}$$

where E_0 denotes the bottom value of the energy spectrum. First for $\lambda = 0$, the system reduces to the attractive Hubbard model. The binding energy $|E_B|/t \sim 0$ in the weak attraction region $U/zt < 1$ ($z = 4$ is the number of the nearest neighbor) and becomes very large for $U/zt \gg 1$, evolving from loosely local pairs (BCS) to tightly bound molecules (BEC) [29]. However, when SOC is added to the lattice, $|E_B|/t$ will be significantly enhanced (left panel of Fig. 3). Note that the states around E_0 mainly contribute to the resonant scattering and the DOS around E_0 is increased by λ; we should have larger value of $|E_B| - 2E_0$ in Eq. (5) to keep the balance of the equation. At the same time, E_0 also increases with λ [see Fig. 1(d)], giving rise to the enhancement of $|E_B|$. In particular, the right panel shows a remarkable growth of $|E_B|/t$ from nearly zero in the weak attraction regions, which signifies the formation of SOC-induced bound states (see $U/t = 2,3$, for example).

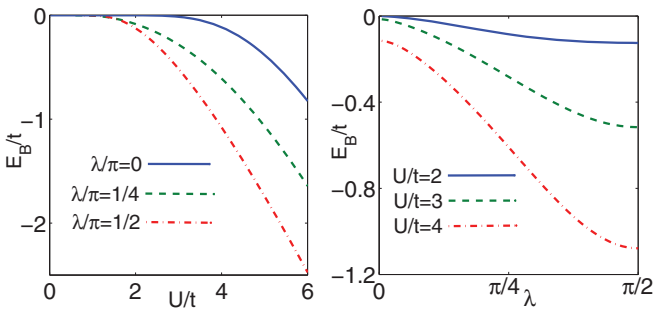

FIG. 3. (Color online) Binding energy E_B/t as a function of U/t (left panel) and strength λ of SOC (right panel).

In general, such an evolution from Dirac superfluidity to the BCS-BEC crossover is the unique feature of the system, where both the SOC and lattices themselves play a fundamental role. Figure 2(c) shows the corresponding chemical potentials. For large fillings, we see that μ decreases with λ due to the formation of Dirac cones. On the other hand, μ is increased unexpectedly for small fillings. This is in contrast with the general arguments that the chemical potentials are always reduced by the bound states in free space. In Fig. 2(d), we plot Δ as a function of U/t. Significantly, we show that strong SOC can remarkably enhance ($n = 0.1$) or suppress ($n = 0.95$) the pairing gaps of the traditional BCS-BEC crossover in the attractive Hubbard model, especially in the weak and intermediate attraction regions. Whereas in the large attraction limit, Δ approaches the $\lambda = 0$ results, in accordance with Eq. (4).

In the above, we have discussed the pairings of the superfluidity at zero temperature. Experimentally, it would be virtually impossible to reach zero temperature. Thus the discussion on finite-temperature phases is much more important. In Figs. 4(a) and 4(b), we plot the gap versus λ at finite temperature T for two typical fillings. We see that the evolution from the Dirac cone dominated superfluidity at high filling to the BCS-BEC crossover at low filling can be clearly observed even at finite temperatures. Furthermore, we present the finite-temperature phase transition at half filling near $\lambda = \pi/2$ in Fig. 4(c). We find that, the system undergoes a normal state to a superfluid state phase transition above a critical value U_c, which approaches the zero temperature semimetal-superfluid QPT point with decreasing temperature.

V. EFFECTS OF SOC ON THE CONDENSATE AND SUPERFLUID DENSITIES IN THE LATTICES

Now, we turn to the investigation of condensate and superfluid densities in the SO-coupled lattices. First, the condensate density $n_c = \frac{1}{N}\sum_{\mathbf{k},\sigma,\sigma'} |\langle \psi_{\mathbf{k}\sigma}\psi_{-\mathbf{k}\sigma'}\rangle|^2$ [38], where the singlet and induced triplet pairing fields $\langle \psi_{\mathbf{k}\uparrow}\psi_{-\mathbf{k}\uparrow}\rangle = -\frac{\Delta}{4}e^{-i\theta_{\mathbf{k}}}\sum_\nu \frac{\nu}{E_{\mathbf{k},\nu}}$ and $\langle \psi_{\mathbf{k}\uparrow}\psi_{-\mathbf{k}\downarrow}\rangle = -\frac{\Delta}{4}\sum_\nu 1/E_{\mathbf{k},\nu}$ with $\theta_{\mathbf{k}} = \arg(\sin k_x + i \sin k_y)$. While for the superfluid density, we impose a phase twist on order parameter $\Delta \to \Delta e^{i\nabla\theta\cdot\vec{r}_j}$ by a local unitary transformation $\psi_j \to \psi_j e^{i\theta(\vec{r}_j)}$. Then, the inverse Green function can be written as $\mathbf{G}^{-1}[\Delta, \nabla\theta] = G^{-1}[\Delta] + \Sigma[\nabla\theta]$. After lengthy but straightforward calculations, we derive a classical XY model $H_{XY} = \frac{1}{2}\mathcal{J}\int d^2\mathbf{r}[(\partial_x\theta)^2 + (\partial_y\theta)^2]$

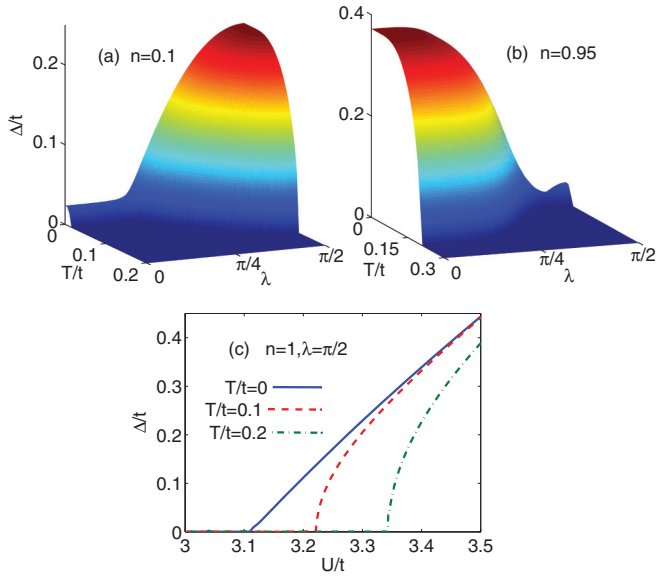

FIG. 4. (Color online) (a), (b) Plot of Δ versus λ at finite temperature T for two typical fillings with $n = 0.1$ (left) and $n = 0.95$ (right), $U/t = 2$. (c) The finite-temperature phase transition of pairing gap as a function of U/t at half filling for $\lambda = \pi/2$. $T/t = 0$ (solid line), 0.1 (dashed line), and 0.2 (dash-dotted line).

with $\mathcal{J}$ the phase stiffness. Therefore, the superfluid density can be defined as $\rho_s = \frac{\mathcal{J}}{2tN}$, which reads

$$\begin{aligned}\rho_s = {} & \frac{\cos\lambda}{N}\sum_{\mathbf{k}}\cos k_x n_{\mathbf{k}} \\ & + \frac{\sin\lambda}{N}\sum_{\mathbf{k},\nu}\frac{\nu\xi_{\mathbf{k},\nu}}{2E_{\mathbf{k},\nu}}\frac{\sin^2 k_x}{\mathcal{K}}\tanh\left(\frac{\beta E_{\mathbf{k},\nu}}{2}\right) \\ & + \frac{2t}{N}\sum_{\mathbf{k},\nu} f'(E_{\mathbf{k},\nu})\sin^2 k_x\left(\cos\lambda + \nu\frac{\sin\lambda\cos k_x}{\mathcal{K}}\right)^2 \\ & - \frac{\sin\lambda}{N}\sum_{\mathbf{k},\nu}\nu\frac{\varepsilon_{\mathbf{k}}^2 + \nu 2t\,\sin\lambda\mathcal{K}\varepsilon_{\mathbf{k}} + \Delta^2}{2\varepsilon_{\mathbf{k}}E_{\mathbf{k},\nu}}\frac{\sin^2 k_y\cos^2 k_x}{\mathcal{K}^3} \\ & \times\tanh\left(\frac{\beta E_{\mathbf{k},\nu}}{2}\right). \qquad (6)\end{aligned}$$

Here $n_{\mathbf{k}} = 1 - \sum_{\nu=\pm}\frac{\varepsilon_{\mathbf{k}}}{2E_{\mathbf{k},\nu}}\tanh(\frac{\beta E_{\mathbf{k},\nu}}{2})$ and the third term vanishes at $T = 0$. Note that, Eq. (6) can give rise to many intriguing features.

Figure 5(a) shows the condensate fraction n_c versus λ for different fillings. First for $n = 0.1$, we see that n_c increases rapidly above a characteristic value λ_c, in accordance with the formation of SOC-induced bound states. The characteristic value λ_c grows with increasing fillings, and until $n \simeq 0.7$, n_c begins to decrease with respect to λ and the BCS superfluidity would be suppressed (see $n = 0.95$, for example). Instead, the superfluid fraction ρ_s is always suppressed by SOC and generally decreases with increasing n, as shown in Fig. 5(b). Significantly, there exhibits a characteristic minimum of λ, which moves rightward when n is increased.

In Figs. 5(c) and 5(d), we plot n_c and ρ_s as a function of U/t. We show that, in the weak and intermediate attraction regions,

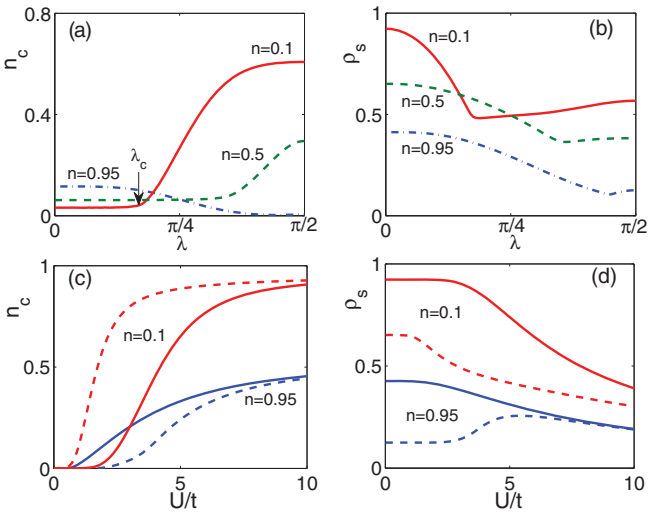

FIG. 5. (Color online) (a) Condensate density n_c and (b) superfluid density ρ_s (both divided by n) at $T = 0$ as a function of λ for different fillings, where we take $U/t = 2$. (c) Plot of n_c and (d) ρ_s versus U/t for two typical fillings with $n = 0.1$ (red) and 0.95 (blue). Solid and dashed lines represent $\lambda = 0$ and $\pi/2$, respectively.

while the condensate fraction is greatly enhanced ($n = 0.1$) or suppressed ($n = 0.95$) by strong SOC in accordance with the pairing gaps, the superfluid fraction always decreases with increasing U/t and λ. Whereas in the large attraction limit, where all the atoms form tightly bound molecules, both n_c and ρ_s will approach the results without SOC.

VI. DISCUSSION AND CONCLUSION

We now discuss some issues related to the experiments. First, the superfluidity discussed in this system is quite different from that induced by a Feshbach resonance [39], where a two-channel model applies. For a broad resonance where the molecular state in the closed channel is negligible, the

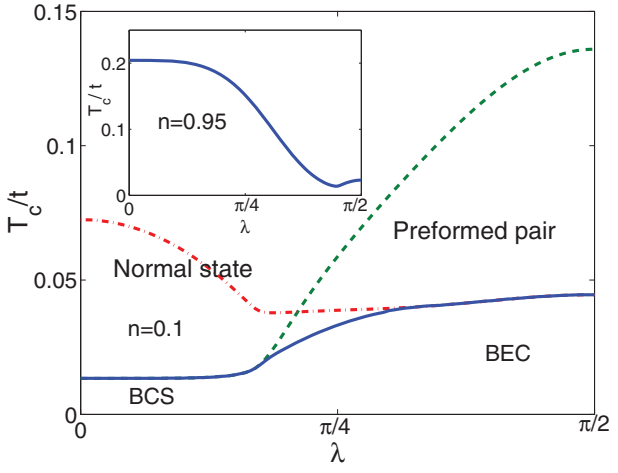

FIG. 6. (Color online) Plot of superfluid transition temperature T_c (solid lines) versus λ for $n = 0.1$ and $n = 0.95$ (inset), $U/t = 2$. The dashed and dash-dotted lines represent the mean-field and KT temperatures, respectively.

optical lattices can be well described by the Hubbard model as the scattering length $a_s \ll a$ (lattice spacing) [21,26,40] or far from the resonance [41,42]. Actually, both the repulsive [23] and attractive [24] Hubbard models have been successfully realized in ^{40}K atoms. Second, many ingenious techniques have been proposed to reach the superfluidity induced by a Hubbard U attraction [11,25]. Recently, exciting advances have been made to approach the antiferromagnetic order [43] or detect the preformed pairs in the attractive Hubbard regime [24]. Finally, we plot the normal-superfluid transition temperature T_c versus λ for two typical fillings in Fig. 6. For $n = 0.95$, T_c is obtained by the mean-field equations and suppressed with increasing SOC. Instead, T_c is considerably enhanced in the strong SOC regime for $n = 0.1$ with KT transition temperature $T_{\mathrm{KT}} = \pi\mathcal{J}/2$.

At finite temperature, the long-range order cannot survive in a two-dimensional system. The low-energy excitations of the "superfluid phases" are bound vortex-antivortex pairs, which are captured by the classical phase variation model of pairing fields. Note that, the derived phase variation model in our system is the usual XY model; while the SOC mainly affects the superfluid stiffness, one can ignore the SOC effects on those bound vortex-antivortex pairs. This differs from the boson gas, where the SOC-induced stripe phase gives rise to much involved phase variations and fractionalized vortices (see Ref. [44], for example).

In conclusion, we have shown that this system displays a variety of emerging physics. The introduction of SOC into the lattices can induce Dirac semimetal and the system undergoes an interesting semimetal-superfluid transition. While upon dopings, the system evolves from the Dirac superfluidity near half filling to the SOC induced BCS-BEC crossover at small fillings, which is characterized by the formation of a novel bound state in the lattices. This system may stimulate more interest in searching new physics beyond the conventional Fermi-Hubbard model in experiments.

ACKNOWLEDGMENTS

We acknowledge Hui Zhai, G. Juzeliūnas, and X. F. Zhang for helpful discussions. We are grateful to Hui Zhai for carefully reading the manuscript. This work is supported by NCET, NSFC under Grants No. 11074175 and No. 10934010, NSFB under Grant No. 1092009, NKBRSFC under Grants No. 2011CB921502 and No. 2012CB821305, and NSFC-RGC under Grant No. 11061160490.

[1] M. Hasan and C. Kane, Rev. Mod. Phys. **82**, 3045 (2010).
[2] X.-L. Qi and S.-C. Zhang, Rev. Mod. Phys. **83**, 1057 (2011).
[3] J. Dalibard, F. Gerbier, G. Juzeliūnas, and P. Öhberg, Rev. Mod. Phys. **83**, 1523 (2011).
[4] Y.-J. Lin, R. L. Compton, K. Jimenez-Garcia, J. V. Porto, and I. B. Spielman, Nature (London) **462**, 628 (2009).
[5] Y.-J. Lin, K. Jiménez-García, and I. B. Spielman, Nature (London) **471**, 83 (2011).
[6] J.-Y. Zhang *et al.*, Phys. Rev. Lett. **109**, 115301 (2012).
[7] P.-J. Wang, Z.-Q. Yu, Z.-K. Fu, J. Miao, L.-H. Huang, S.-J. Chai, H. Zhai, and J. Zhang, Phys. Rev. Lett. **109**, 095301 (2012).
[8] L. W. Cheuk, A. T. Sommer, Z. Hadzibabic, T. Yefsah, W. S. Bakr, and M. W. Zwierlein, Phys. Rev. Lett. **109**, 095302 (2012).
[9] T. D. Stanescu, B. Anderson, and V. Galitski, Phys. Rev. A **78**, 023616 (2008).
[10] C. Wang, C. Gao, C.-M. Jian, and H. Zhai, Phys. Rev. Lett. **105**, 160403 (2010).
[11] T.-L. Ho and S.-Z. Zhang, Phys. Rev. Lett. **107**, 150403 (2011).
[12] S. Sinha, R. Nath, and L. Santos, Phys. Rev. Lett. **107**, 270401 (2011).
[13] M. Iskin and A. L. Subasi, Phys. Rev. Lett. **107**, 050402 (2011).
[14] J. P. Vyasanakere, S. Zhang, and V. B. Shenoy, Phys. Rev. B **84**, 014512 (2011); J. P. Vyasanakere and V. B. Shenoy, *ibid.* **83**, 094515 (2011).
[15] H. Hu, L. Jiang, X.-J. Liu, and H. Pu, Phys. Rev. Lett. **107**, 195304 (2011).
[16] Z.-Q. Yu and H. Zhai, Phys. Rev. Lett. **107**, 195305 (2011).
[17] M. Gong, S. Tewari, and C. Zhang, Phys. Rev. Lett. **107**, 195303 (2011).
[18] L. Han and C. A. R. Sáde Melo, Phys. Rev. A **85**, 011606(R) (2012).
[19] K. Zhou and Z. Zhang, Phys. Rev. Lett. **108**, 025301 (2012).
[20] L. He and X.-G. Huang, Phys. Rev. Lett. **108**, 145302 (2012).
[21] T. Esslinger, Annu. Rev. Condens. Matter Phys. **1**, 129 (2010).
[22] I. Bloch, J. Dalibard, and W. Zwerger, Rev. Mod. Phys. **80**, 885 (2008).
[23] R. Jördens, N. Strohmaier, K. Günter, H. Moritz, and T. Esslinger, Nature (London) **455**, 204 (2008); U. Schneider, L. Hackermüller, S. Will, Th. Best, I. Bloch, T. A. Costi, R. W. Helmes, D. Rasch, and A. Rosch, Science **322**, 1520 (2008).
[24] L. Hackermüller, U. Schneider, M. Moreno-Cardoner, T. Kitagawa, Th. Best, S. Will, E. Demler, E. Altman, I. Bloch, and B. Paredes, Science **327**, 1621 (2010); U. Schneider *et al.*, Nat. Phys. **8**, 213 (2012).
[25] W. Hofstetter, J. I. Cirac, P. Zoller, E. Demler, and M. D. Lukin, Phys. Rev. Lett. **89**, 220407 (2002).
[26] A. F. Ho, M. A. Cazalilla, and T. Giamarchi, Phys. Rev. A **79**, 033620 (2009).
[27] T. Paiva, R. Scalettar, M. Randeria, and N. Trivedi, Phys. Rev. Lett. **104**, 066406 (2010).
[28] L. Salasnich and F. Toigo, Phys. Rev. A **86**, 023619 (2012).
[29] For a review of attractive Hubbard model, see R. Micnas, J. Ranninger, and S. Robaszkiewucz, Rev. Mod. Phys. **62**, 113 (1990).
[30] J. Radić, A. Di Ciolo, K. Sun, and V. Galitski, Phys. Rev. Lett. **109**, 085303 (2012).
[31] W. S. Cole, S. Zhang, A. Paramekanti, and N. Trivedi, Phys. Rev. Lett. **109**, 085302 (2012).
[32] T. Graß, K. Saha, K. Sengupta, and M. Lewenstein, Phys. Rev. A **84**, 053632 (2011).
[33] N. Goldman, A. Kubasiak, A. Bermudez, P. Gaspard, M. Lewenstein, and M. A. Martin-Delgado, Phys. Rev. Lett. **103**, 035301 (2009).
[34] In this work, we shall focus on the "basic region" given by $\lambda \in [0,\pi/2]$, because the relevant physical results are not affected in other regions.

[35] K. Osterloh, M. Baig, L. Santos, P. Zoller, and M. Lewenstein, Phys. Rev. Lett. **95**, 010403 (2005).
[36] S. Robaszkiewicz, R. Micnas, and K. A. Chao, Phys. Rev. B **23**, 1447 (1981).
[37] Strictly speaking, for half filling with $\bar{\mu} = 0$, the superfluid state is degenerate with charge density wave state in H_{spin}.
[38] L. P. Gor'kov and E. I. Rashba, Phys. Rev. Lett. **87**, 037004 (2001).
[39] J. K. Chin, D. E. Miller, Y. Liu, C. Stan, W. Setiawan, C. Sanner, K. Xu, and W. Ketterle, Nature (London) **443**, 961 (2006).
[40] D. Jaksch, C. Bruder, J. I. Cirac, C. W. Gardiner, and P. Zoller, Phys. Rev. Lett. **81**, 3108 (1998).
[41] R. B. Diener and T.-L. Ho, Phys. Rev. Lett. **96**, 010402 (2006).
[42] T.-L. Ho and Q. Zhou, Proc. Natl. Acad. Sci. USA **106**, 6916 (2010); M. Popp, J. J. Garcia-Ripoll, K. G. Vollbrecht, and J. I. Cirac, Phys. Rev. A **74**, 013622 (2006); J. S. Bernier, C. Kollath, A. Georges, L. DeLeo, F. Gerbier, C. Salomon, and M. Kohl, *ibid*. **79**, 061601 (2009).
[43] P. Medley, D. M. Weld, H. Miyake, D. E. Pritchard, and W. Ketterle, Phys. Rev. Lett. **106**, 195301 (2011).
[44] C.-M. Jian and H. Zhai, Phys. Rev. B **84**, 060508(R) (2011).